CCC 2025 **Proceedings of the Creative Construction Conference** (2025)
Edited by: Miroslaw J. Skibniewski & Miklós Hajdu & Žiga Turk
https://doi.org/10.22260/CCC2025/0069

ASSESSMENT OF SELF COMPACTING CONCRETE PARAMETERS BY IMAGE ANALYSIS

Önder Halis Bettemir, Kâzım Türk
İnönü University, Malatya, Türkiye

Abstract

Self-compacting concrete (SCC) with multi blended fiber reinforcement is widely used in earthquake zones. However, workability tests of the SCC are susceptible to human error and time consuming to assess. In this study, image analysis techniques are utilized to assess the filling ability, passing ability, and segregation resistance tests of SCC without human intervention. A steel frame is constructed to assemble two digital optic cameras with calibrated interior and exterior orientation parameters to obtain stereo images of the tested SCC. The flow radius of the SCC is detected by binarization with Otsu threshold method to eliminate any necessity of expert opinion to conduct the evaluation process. The flow time of SCC within 500 mm radius is detected by sampling 0.1 Hz frequent images. Moreover, the slump value is measured better than sub-millimeter accuracy by the help of stereo imaging. Duration of flow-through test from O-funnel or V-funnel is measured accurately by the developed stereo imaging technique and implementing binarization with Otsu threshold. The proposed system is also implemented for the assessment of L-type flow tester and measured the leveling time of the SCC more accurately than human. Furthermore, if the SCC specimen cannot reach the maximum level distance, the obtained level distance is also measured accurately. The maximum distance that SCC reached is detected by binarization with Otsu threshold then the stereo images are obtained and the position and height of the SCC is measured from the coupled binary images. The stereo camera is positioned to capture only the test apparatus with minimum background objects to ensure successful binarization. Pre-calibration of the optic images ensures correct matching of the overlapping ground points. Consequently, successful results are obtained from the laboratory tests. Automated assessment of SCC test can be helpful for SCC producers to evaluate the properties of their products correctly.

Keywords: stereo imaging, Otsu threshold, self-compacting concrete, binarization.

Peer-review under responsibility of the scientific committee of the Creative Construction Conference 2025.

1. Introduction

1.1. Self-compacting concrete

Building Codes for Reinforced Concrete Structures require placement of more stirrups and ties at the column-beam joints for the buildings to be constructed at earthquake zones. Proper placement of concrete where the amount of reinforcement is dense becomes very difficult. Therefore, Self Compacting Concrete (SCC) is developed by Okamura to solve the aforementioned problem [1]. SCC can pass between the dense reinforcements and fill the formwork with its own weight without vibration requirement. Therefore it is widely used at the reinforced concrete buildings that are located at regions vulnerable to destructive earthquakes. On the other hand, workability test of SCC is different than conventional concrete.

Workability tests defined in EFNAC (2005) (slump-sprawl, T500, VSI, J-ring and L-box tests) are applied on the designed fresh SCC mixtures. As a result of the workability tests, the limit values determined by EFNARC (2002) and presented in Table 1 are taken as basis.

Table 1. Acceptance criteria for SCC (EFNARC, 2002)

Corresponding author email address: onder.bettemir@inonu.edu.tr

Method	Unit	Minimum	Maximum
Slump test with Abrahams Cone	mm	650	800
T500mm	second	2	5
J-ring	Mm	0	10
L-box	h2/h1	0.8	1.0

Slump test and T500 test are conducted using spreading table and truncated cone apparatus as shown in Figure 1.

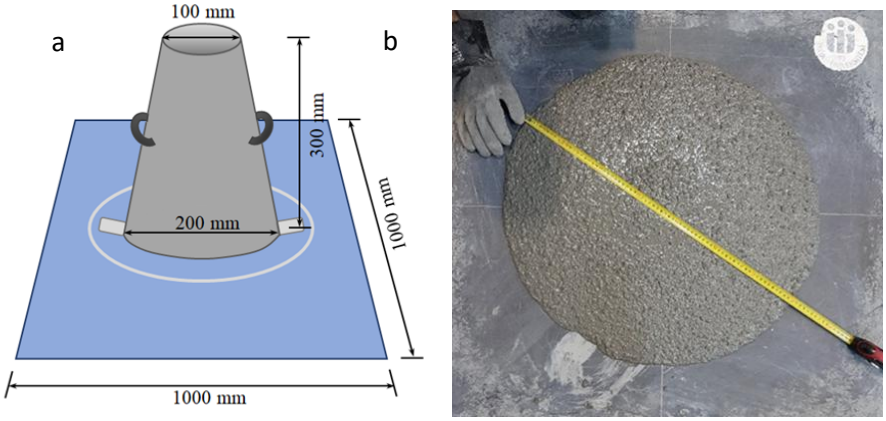

Fig. 1. (a) standard slump cone; (b) Measurement of the spread of SCC.

The J-ring test setup presented in Figure 2 is used to determine the ability of the SCC mixture to pass through obstacles and level out during workability tests.

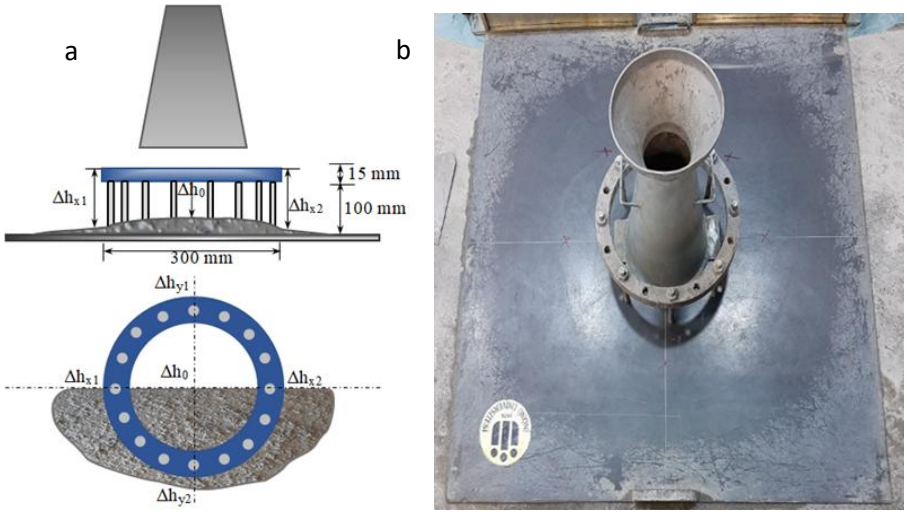

Fig. 2. (a) J-ring test drawings; (b) J-ring test apparatus.

Duration of the flow of concrete between the bars and the amount of spread of the concrete are measured manually as given in Fig. 1 in order to evaluate that the produced concrete satisfy the requirements given in Table 1. The experiments are conducted on concrete which is intended to be SCC. Measurement of the spread of the concrete at a specific time or the measurement of the time when the concrete reaches a particular spread amount becomes error prone as the concrete is highly fluid. Therefore, aforementioned difficulties motivated the authors to develop an automated visual system which can assess the suitability of the concrete for the EFNARC criteria.

Besides the difficulties of the workability tests, transportation of SCC from the ready mix concrete plant to construction site may cause differences in the properties of the concrete if the duration of transport

increases. This may cause very difficult conflicts to solve between the material supplier and the contractor since the execution of the tests are error prone; test procedure involves no official recording, and the phenomenon to be measured changes in a very short time without giving any opportunity to be evidence. The recorded visual images and the image analysis results can also be utilized as evidence to resolve any disputes.

1.2. Literature review

Image analysis and artificial intelligence are frequently utilized to predict the mechanical properties of hardened concrete. Vlahovic et al. [2] utilized Image Pro Plus software to conduct image analysis for acid resistance testing. The surface destruction and the damaged surface were monitored by image analysis. Lemaire et al. [3] utilized image analysis to detect surface holes on the concrete elements. In order to normalize illumination effects the images are subjected to contrast enhancement and median threshold filtering to remove noises. The image is binarized by the threshold value obtained by maximum entropy; the binary image is subjected to morphologic opening to detect air bubbles on the concrete surface. Han et al. [4] utilized image analysis to detect the aggregate size and distribution of concrete specimen. Otsu threshold algorithm is utilized in order to obtain the value of the threshold to distinguish the aggregates from the cement. Fritz et al. [5] visualized the position and orientation of steel fibers as well as the roundness of the particles in concrete. The study aimed to visualize the results of Non-Destructive Test methods. Zheng et al. [6] utilized segmenting objects by Locations Version 2 (SoloV2) toolbox which is an instance segmentation network. Utilized toolbox segmented the coarse aggregates by digital image analysis and morphology of the coarse aggregates are retrieved.

Arunachalam and Henderson [7] implemented artificial neural network (ANN) to estimate the compressive strength of prefabricated concrete bricks. ImageJ software is utilized for image cropping and conversion from RGB to grey scale images. Then image arithmetic obtained from the ImageJ software is fed to the ANN. Dogan et al. [8] utilized ANN fed by digital images of concrete specimens to predict compressive strength.

Wang et al. [9] determined the mortar-to-coarse aggregate ration and inter-particle spacing between coarse aggregate by digital image processing conducted on MATLAB. Images of hardened concrete are converted from RGB to grey scale image and Otsu threshold algorithm is implemented for binarization to extract coarse aggregate. Torrijos [10] implemented image analysis to determine coarse aggregate distribution as well as distribution of the fibres. Fonseca and Scherer [11] painted concrete samples with a thin layer of black acrylic ink and utilized fine white barium sulphate powder to fill the voids. Flatbed scanner with 3200 dpi resolution is used to acquire digital images of the concrete specimens. Otsu's method of thresholding is implemented to detect the amount of air voids. Liu et al. [12] utilized Image J software to determine the porosity of concrete specimens with digital image analysis. The images of the concrete specimens are binarized by threshold operation conducted by the Image J software.

Image J software was utilized to assess the correlation between the aggregate morphology and the mechanical properties of asphalt concrete. RGB images of asphalt concrete were converted to grey scale images and then binarized with global thresholding [13, 14]. Soroushian and Elzafraney [15] executed dilation, erosion, opening, closing, and hole-fill image processing operations on environmental scanning electron and microscopy images of concrete specimens. Voids and micro-cracks are detected by image analysis. Qi et al. detected shrinkage cracks on concrete specimens. In order to obtain binary image 80% of the value of the peak frequency is assigned as threshold value. The pores in the binary images were cleaned by Photoshop software. The image is filtered by a low pass open filter to improve image quality [16]. Mazzoli et al. [17] implemented image analysis to evaluate shrinkage cracks. AutoStitch was utilized to merge images of concrete specimens. Image J software was utilized to analyse the sizes of the cracks including width, length, and area properties.

Literature review revealed that assessment of workability parameters of self-compacting concrete by digital image analysis has not been conducted yet. This study aims to fulfil the addressed literature gap and aims to detect the slump and spread of fresh self-compacting concrete with image analysis.

2. Methodology

The threshold value assignment method proposed by Otsu aims to determine a threshold value to separate the image into two classes as background and examined object. The threshold value is determined by maximizing the averages of the image values that constitute the background and the object. The computational procedure assumes the existence of L grey levels in the image and the number of picture elements that have brightness level of i where i = 1,…,L is shown as n_1, n_2, …, n_L. In this representation it is seen that $n_1 + n_2 + \ldots + n_L = N$ where N is the number of picture elements that constitute the image. The probability of a picture element being at the i^{th} brightness level is represented by Eq. 1.

$$P_i = \frac{n_i}{N} \tag{1}$$

When the threshold value is equal to k, the pixels having the brightness levels [1, 2,…, k] will be classified into class S_0 and the pixels having the brightness levels [k+1, …, L-1, L] will belong to class S_1. Probabilities of a picture element being a member of S_0 and S_1 classes are given in Eq. 2 [18].

$$w_0 = \Pr(S_0) = \sum_{i=1}^{k} P_i = w(k), \quad w_1 = \Pr(S_1) = \sum_{i=k+1}^{L} P_i = 1 - w(k) \tag{2}$$

In Eq. 2 w_0 expresses the probability that any pixel in the image has a brightness value between 1 and k. This value is the probability that the relevant pixel belongs to the S_0 class. The brightness values of the image elements included in the class are presented in Eq. 3.

$$\mu_0 = \sum_{i=1}^{k} \left(i * \Pr(i \mid S_0)\right) = \sum_{i=1}^{k} \left(i * \frac{P_i}{w_0} \right) = \frac{\mu(k)}{w(k)} \tag{3}$$

In Eq. 3 $\mu(k)$, is computed by $\sum_{i=1}^{k} i * P_i$; $w(k)$ is computed by $\sum_{i=1}^{k} P_i$. Average of class S_1 is computed by $\mu_1 = \sum_{i=1+k}^{L} \left(i * \Pr(i \mid S_1)\right) = \sum_{i=k+1}^{L} \left(i * \frac{P_i}{w_1} \right) = \frac{\mu_T - \mu(k)}{1 - w(k)}$. For μ_T ; $\mu_T = \mu(L) = \sum_{i=1}^{L} i * P_i$ equation is valid. Variance of class S_0 is computed by Eq. 4.

$$\sigma_0^2 = \sum_{i=1}^{k} (1 - \mu_0)^2 \Pr(i \mid S_0) = \sum_{i=1}^{k} (1 - \mu_0)^2 \frac{P_i}{w_0} \tag{4}$$

Variance of class S1 is computed by $\sigma_1^2 = \sum_{i=k+1}^{L} (1 - \mu_1)^2 \frac{P_i}{w_1}$. The variance difference between the two classes whose value is desired to be maximized is calculated with the expression presented in Eq. 5.

$$\sigma_B^2(k) = \frac{[\mu_T w(k) - \mu(k)]^2}{w(k)[1 - w(k)]} \tag{5}$$

The maximum value of the objective function is calculated by assigning all possible k values from 1 to 255 in the eight-bit image and calculating the variance differences. The maximum value of the objective function calculated using Eq. 5 according to the assigned k value is calculated as a result of 256 trials.

3. Methodology

Detection of the spread of the concrete by image analysis is examined by the image illustrated in Figure 3.a. The test image illustrates the image of SCC after conducting the slump test on the spread table. The table is used numerous times and its surface is covered by mortar residues which simulates the actual case which would be faced at the construction site. The background of the spread table has numerous scratches and has many edges. Moreover, the colour of the background and the SCC is not significantly different. Moreover, fibers inside the SCC and the aggregate will create many edges.

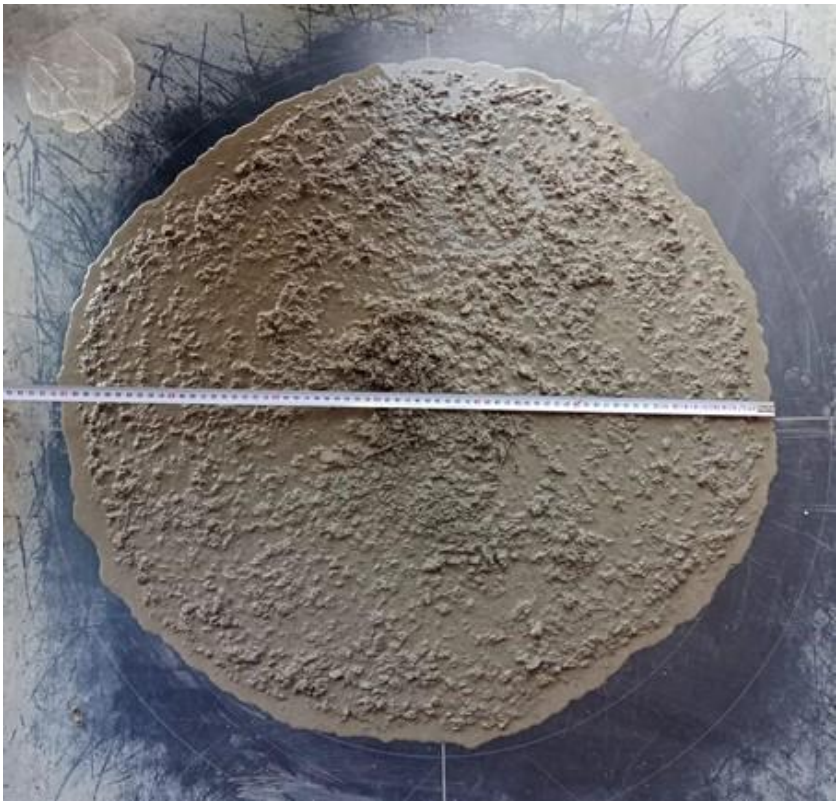

Fig. 3. Sample spread test image.

In Figure 4.a edge image obtained by Canny edge detection algorithm is presented. The edge image is binarized by Otsu threshold and the resulting image is shown in Figure 4.b. In Figures 4.c to 4.g binary images obtained by contrast binarization method with 15, 25, 49, 81, and 121 pixel kernel size, respectively. Figure 4.h represents the edge image obtained by Frei-Chen edge detection and the binary image obtained by Otsu threshold is given in Figure 4.ı. Figure 4.i illustrates the edge image obtained by integrated function analysis and the binary image obtained by Otsu threshold is shown in Figure 4.j. Figure 4.k demonstrates the edge image obtained by Kirsch edge operator and the binary image obtained by Otsu threshold is illustrated in Figure 4.l. Figure 4.m represents the edge image obtained by First Order Laplace edge operator and the binary image obtained by Otsu threshold is given in Figure 4.n. Figure 4.o represents the edge image obtained by Second Order Laplace edge operator and the binary image obtained by Otsu threshold is given in Figure 4.ö. . In Figures 4.p to 4.t binary images obtained by median binarization method with 7, 15, 25, 49, and 81 pixel kernel size, respectively. Figure 4.u represents the edge image obtained by Modified Frei-Chen edge detection and the binary image obtained by Otsu threshold is given in Figure 4.w. Figure 4.x represents the edge image obtained by the second Modification of Frei-Chen edge detection and the binary image obtained by Otsu threshold is given in Figure 4.y. In Figures 4.z to 4.ad binary images obtained by mean binarization method with 7, 15, 25, 49, and 81 pixel kernel size, respectively. Figure 4.ae illustrates the binary image obtained by direct Otsu threshold. Figure 4.af represents the edge image obtained by Prewitt edge operator and the binary image obtained by Otsu threshold is given in Figure 4.ag. Figure 4.ah represents the edge image obtained by Roberts edge operator and the binary image obtained by Otsu threshold is given in Figure

4.ai. Figure 4.aj represents the edge image obtained by Robinson edge operator and the binary image obtained by Otsu threshold is given in Figure 4.ak. Figure 4.al represents the edge image obtained by Sobel edge operator and the binary image obtained by Otsu threshold is given in Figure 4.am.

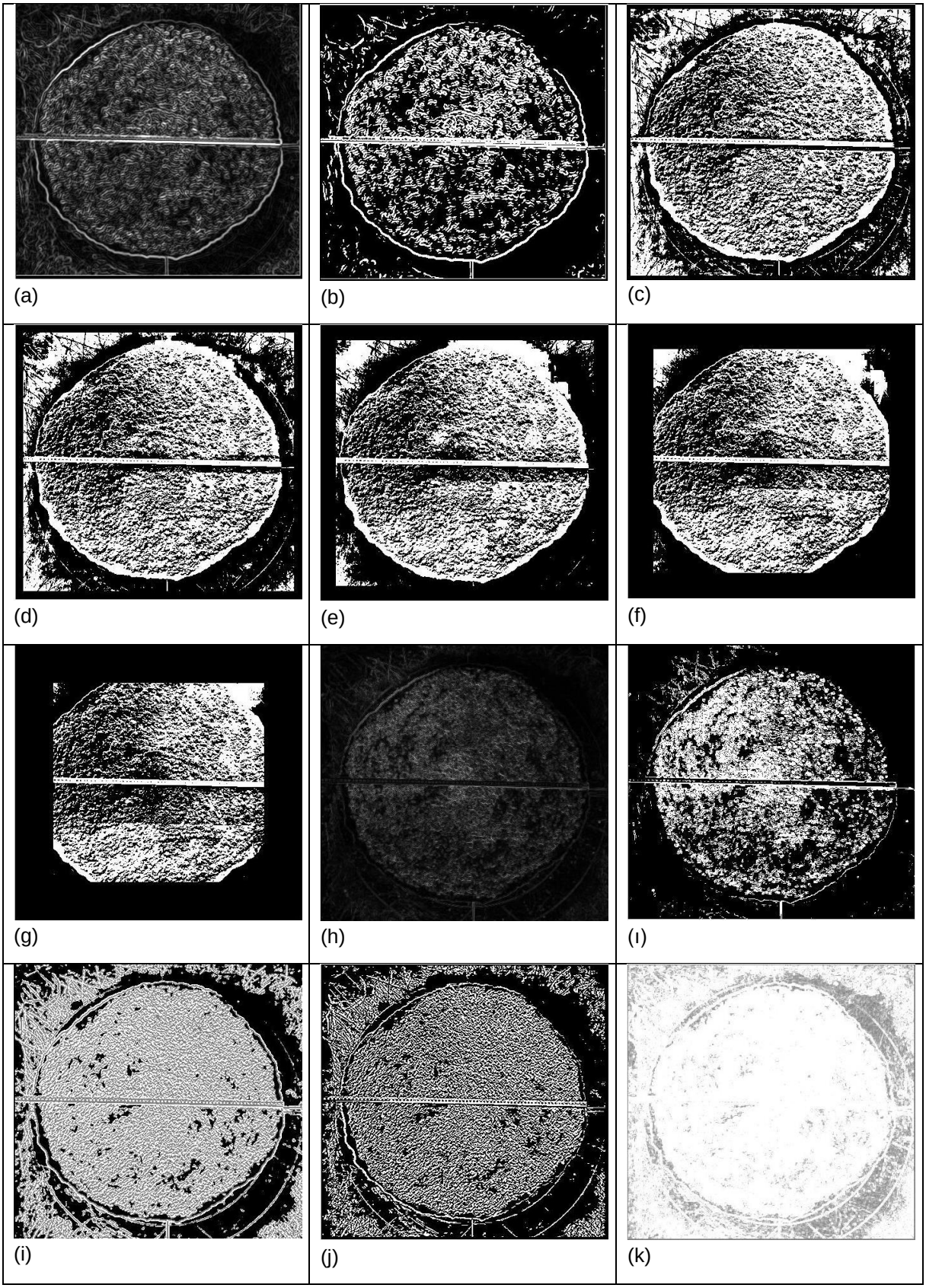

(a) (b) (c)

(d) (e) (f)

(g) (h) (ı)

(i) (j) (k)

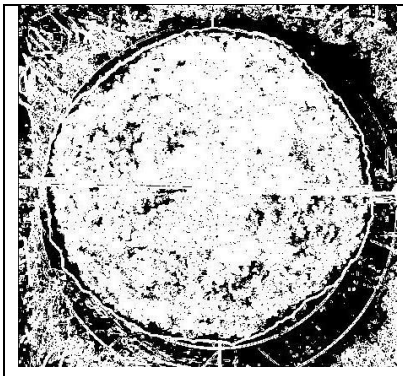

(l)

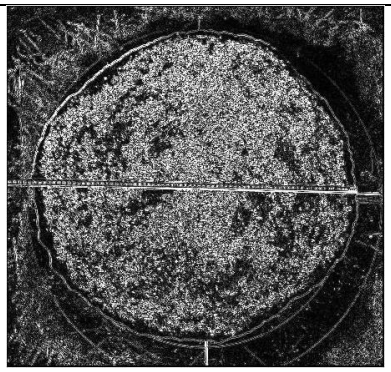

(m)

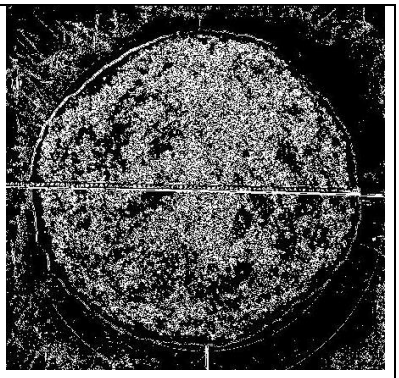

(n)

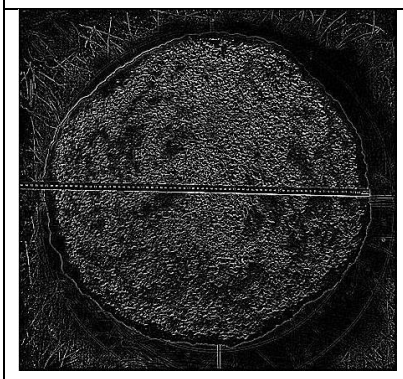

(o)

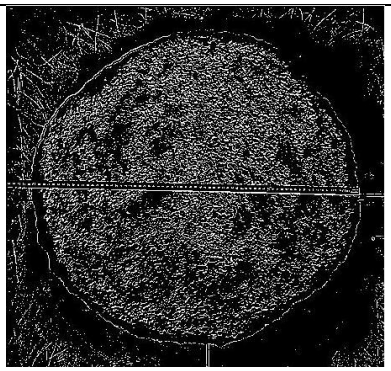

(ö)

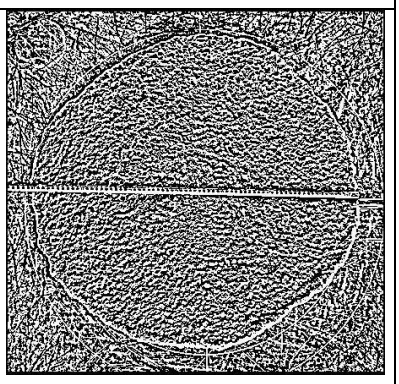

(p)

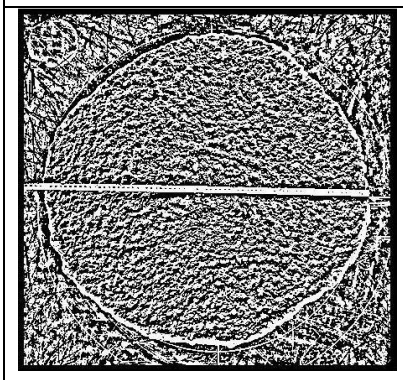

(q)

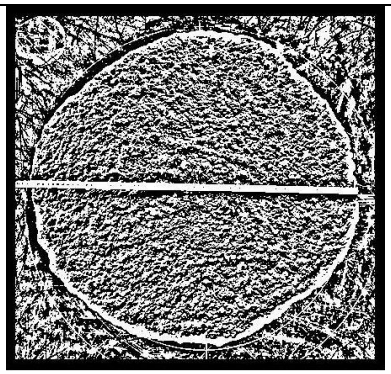

(r)

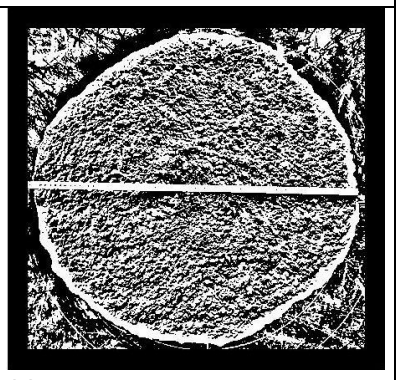

(s)

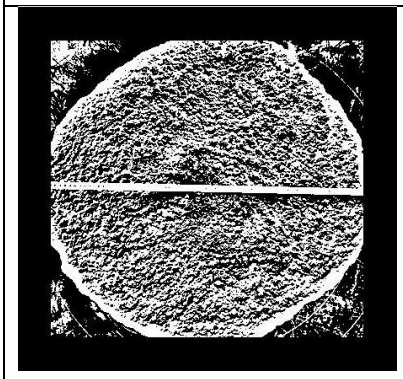

(t)

(u)

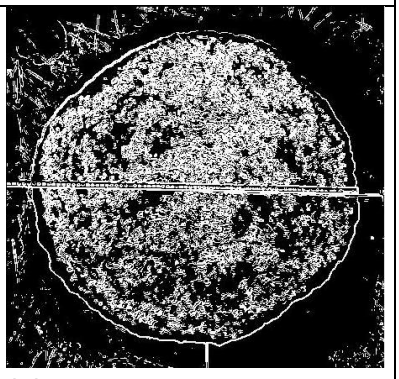

(w)

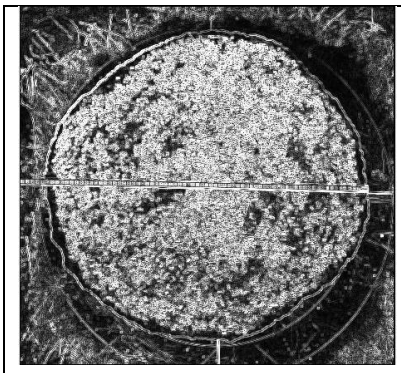

(x)

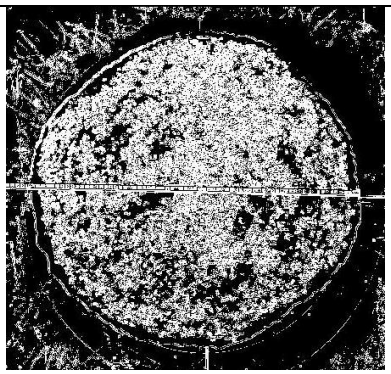

(y)

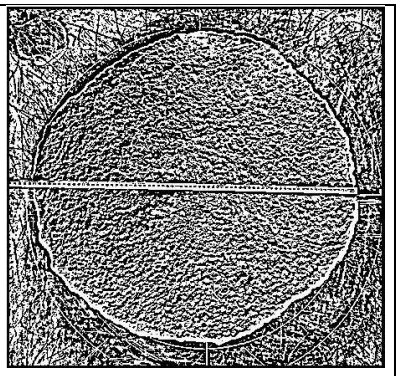

(z)

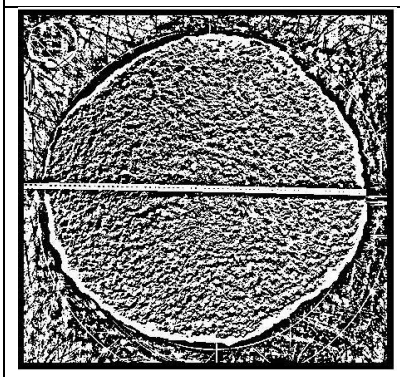

(aa)

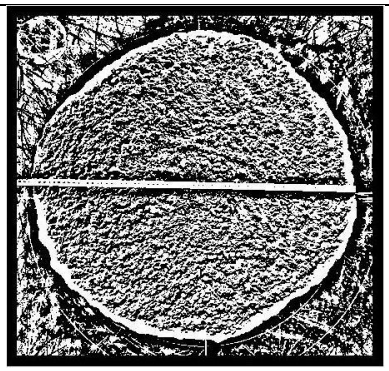

(ab)

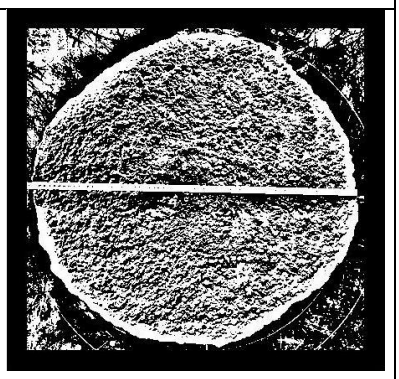

(ac)

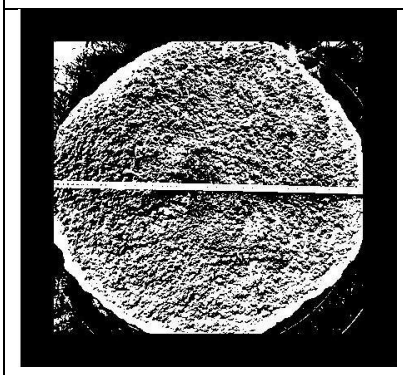

(ad)

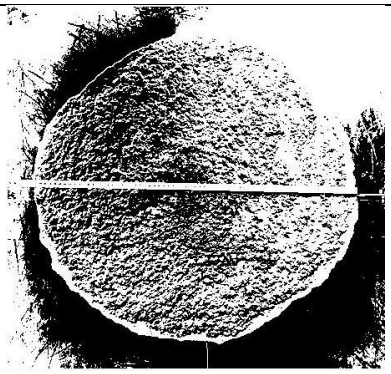

(ae)

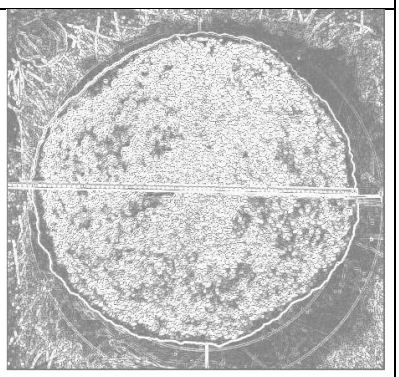

(af)

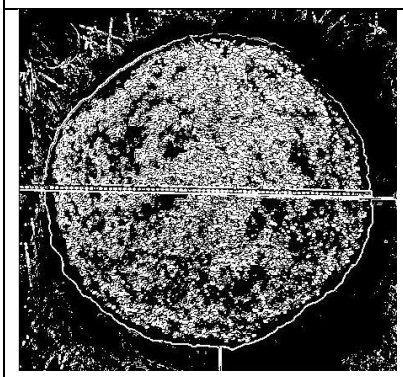

(ag)

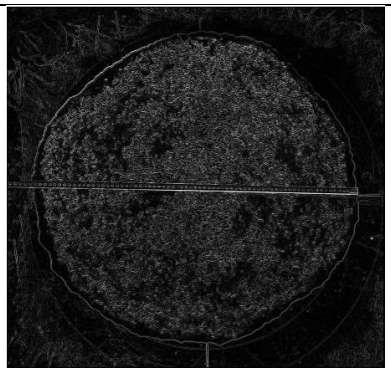

(ah)

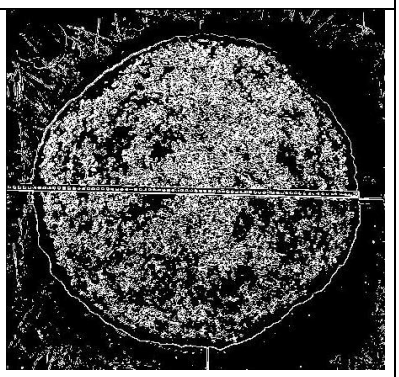

(ai)

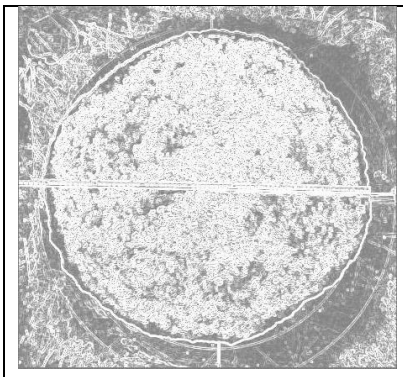 (aj)	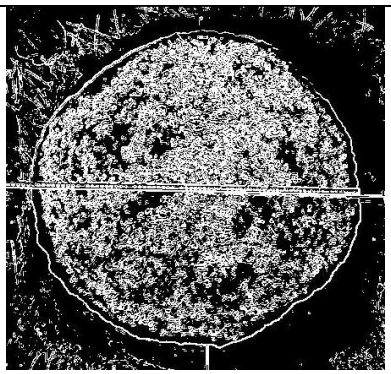 (ak)	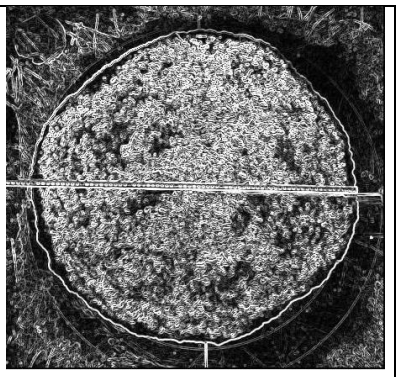 (al)
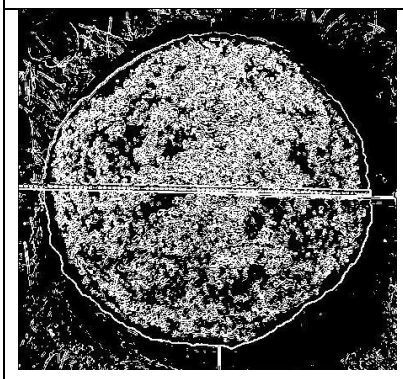 (am)		

4. Discussion and Conclusion

The listed edge and binary images are examined visually. It is concluded that Canny edge detection and Otsu pair (Fig. 4.a and Fig. 4.b) provides good results. First modification of Frei-Chen (4.u and 4.w), second modification of Frei-Chen (4.x and 4.y), Prewitt (4.af and 4.ag), and Roberts (4.ah and 4.ai) provide good results which can be considered for photogrammetric measurements. Contrast binary operator for 81 and 121 kernel size (Fig.4e and Fig.4f), integrated functional analysis (Fig 4.i and Fig.4j), Kirsch edge operator (Fig 4.k and 4.l), First order Laplace operator (Fig 4.m and 4.n), Second order Laplace operator (Fig.4o-ö), Median binary operator with 25 and 49 kernel size (Fig.4.s-t), Mean binary operator with 49 and 81 kernel size (Fig 4.ac and 4.ad), Robinson edge operator (Fig 4.aj and 4.ak), and Sobel edge operator (Fig 4.am) provided acceptable results. However, these operators are not proposed to be utilized since wrong results may be obtained.

This study revealed the edge operators that can be utilized for the detection of the spread of the self-compacting concrete. The obtained results will be utilized to analyse spread video of SCC in order to assess EFNARC workability tests with digital image analysis and photogrammetric measurements. The initial results of the study revealed that the Canny, Frei-Chen, Prewitt, and Robert operators can be implemented. However, more tests should be conducted by utilizing more spread tests with SCC.

Acknowledgements

This study is supported by the Coordination of Scientific Research Projects of İnönü University by the grant no FBA-2025-3917.

References

[1] Okamura H. Self compacting high performance concrete– ferguson lecture for 1996. Concr Int 1997;19(7):50–4.

[2] M. M. Vlahović, M. M. Savić, S. P. Martinović, T. Đ. Boljanac, and T. D. Volkov-Husović, “Use of image analysis for durability testing of sulfur concrete and Portland cement concrete,” Materials & Design, vol. 34, pp. 346–354, Feb. 2012, doi: 10.1016/j.matdes.2011.08.026.

[3] G. Lemaire, G. Escadeillas, and E. Ringot, “Evaluating concrete surfaces using an image analysis process,” Construction and Building Materials, vol. 19, no. 8, pp. 604–611, Oct. 2005, doi: 10.1016/j.conbuildmat.2005.01.025.

[4] J. Han, K. Wang, X. Wang, and P. J. M. Monteiro, “2D image analysis method for evaluating coarse aggregate characteristic and distribution in concrete,” Construction and Building Materials, vol. 127, pp. 30–42, Nov. 2016, doi: 10.1016/j.conbuildmat.2016.09.120.
[5] L. Fritz, M. Hadwiger, G. Geier, G. Pittino, and M. E. Groller, “A Visual Approach to Efficient Analysis and Quantification of Ductile Iron and Reinforced Sprayed Concrete,” IEEE Transactions on Visualization and Computer Graphics, vol. 15, no. 6, pp. 1343–1350, Nov. 2009, doi: 10.1109/tvcg.2009.115.
[6] W. Zheng, Z. Shui, Z. Xu, X. Gao, and K. Gao, “Impact of coarse aggregate morphology and separation distance on concrete properties based on visual learning,” Journal of Building Engineering, vol. 89, p. 109254, Jul. 2024, doi: 10.1016/j.jobe.2024.109254.
[7] K. P. Arunachalam and J. H. Henderson, “Experimental Study on Mechanical Strength of Vibro-Compacted Interlocking Concrete Blocks Using Image Processing and Microstructural Analysis,” Iranian Journal of Science and Technology, Transactions of Civil Engineering, vol. 47, no. 6, pp. 3571–3589, Jul. 2023, doi: 10.1007/s40996-023-01194-8.
[8] G. Dogan, M. H. Arslan, and M. Ceylan, “Concrete compressive strength detection using image processing based new test method,” Measurement, vol. 109, pp. 137–148, Oct. 2017, doi: 10.1016/j.measurement.2017.05.051.
[9] X. Wang, K. Wang, J. Han, and P. Taylor, “Image analysis applications on assessing static stability and flowability of self-consolidating concrete,” Cement and Concrete Composites, vol. 62, pp. 156–167, Sep. 2015, doi: 10.1016/j.cemconcomp.2015.05.002.
[10] M. C. Torrijos, B. E. Barragán, and R. L. Zerbino, “Physical–mechanical properties, and mesostructure of plain and fibre reinforced self-compacting concrete,” Construction and Building Materials, vol. 22, no. 8, pp. 1780–1788, Aug. 2008, doi: 10.1016/j.conbuildmat.2007.05.008.
[11] P. C. Fonseca and G. W. Scherer, “An image analysis procedure to quantify the air void system of mortar and concrete,” Materials and Structures, vol. 48, no. 10, pp. 3087–3098, Aug. 2014, doi: 10.1617/s11527-014-0381-9.
[12] R. Liu et al., “Influence of Pore Structure Characteristics on the Mechanical and Durability Behavior of Pervious Concrete Material Based on Image Analysis,” International Journal of Concrete Structures and Materials, vol. 14, no. 1, Jun. 2020, doi: 10.1186/s40069-020-00404-1.
[13] S. Arasan, E. Yenera, F. Hattatoglu, S. Hinislioglua, and S. Akbuluta, “Correlation between Shape of Aggregate and Mechanical Properties of Asphalt Concrete,” Road Materials and Pavement Design, vol. 12, no. 2, pp. 239–262, Jun. 2011, doi: 10.3166/rmpd.12.239-262.
[14] R. Polat, M. M. Yadollahi, A. E. Sagsoz, S.Arasan, “The correlation between aggregate shape and compressive strength of concrete: Digital image processing approach.” Int. J. Struct. Civ. Eng. Res, 2(3), 63-80, 2013, "the referenced item does not yet have a DOI number."
[15] P. Soroushian and M. Elzafraney, “Morphological operations, planar mathematical formulations, and stereological interpretations for automated image analysis of concrete microstructure,” Cement and Concrete Composites, vol. 27, no. 7–8, pp. 823–833, Aug. 2005, doi: 10.1016/j.cemconcomp.2004.07.008.
[16] C. Qi, J. Weiss, J. Olek “Characterization of plastic shrinkage cracking in fiber reinforced concrete using image analysis and a modified Weibull function,” Materials and Structures, vol. 36, no. 260, pp. 386–395, Nov. 2005, doi: 10.1617/12686.
[17] A. Mazzoli, S. Monosi, and E. S. Plescia, “Evaluation of the early-age-shrinkage of Fiber Reinforced Concrete (FRC) using image analysis methods,” Construction and Building Materials, vol. 101, pp. 596–601, Dec. 2015, doi: 10.1016/j.conbuildmat.2015.10.090.